Application of CFE/POST2 for Simulation of Launch Vehicle Stage Separation

Bandu N. Pamadi,* Paul V. Tartabini,† Mathew D. Toniolo,‡
Carlos M. Roithmayr,§ Christopher Karlgaard,** and Jamshid Samareh††
NASA Langley Research Center, Hampton VA 23681

The constraint force equation (CFE) methodology provides a framework for modeling constraint forces and moments acting at joints that connect multiple vehicles. With implementation in Program to Optimize Simulated Trajectories II (POST2), the CFE provides a capability to simulate end-to-end trajectories of launch vehicles, including stage separation. In this paper, the CFE/POST2 methodology is applied to the Shuttle-SRB separation problem as a test and validation case. The CFE/POST2 results are compared with STS-1 flight test data.

Nomenclature

A	=	axial location of the SRB reference point in SSME plume coordinate system
a_x, a_y, a_z	=	acceleration components along body axes (excluding components due to gravity) ft/sec^2
C_A	=	axial force coefficient
ΔC_A	=	incremental (proximity) axial force coefficient
C_l	=	rolling moment coefficient
ΔC_l	=	incremental (proximity) rolling moment coefficient
C_m	=	pitching moment coefficient
ΔC_m	=	incremental (proximity) pitching moment coefficient
C_N	=	normal force coefficient
ΔC_N	=	incremental (proximity) normal force coefficient
C_n	=	yawing moment coefficient
ΔC_n	=	incremental (proximity) yawing moment coefficient
C_Y	=	side force coefficient
ΔC_Y	=	incremental (proximity) side force coefficient
F_x, F_y, F_z	=	aerodynamic forces in axial, lateral and normal directions, lb
$\mathbf{F}_A^{(CON)}, \mathbf{F}_B^{(CON)}$	=	Joint constraint force vector for body A, and B
$\mathbf{F}_A^{(EXT)}, \mathbf{F}_B^{(EXT)}$	=	External force vector acting on body A, and B
h	=	altitude, ft
i	=	variable index
I_{xx}, I_{yy}, I_{zz}	=	moment of inertia about body x, y, and z axes, slugs ft^2
I_{xy}, I_{yz}, I_{zx}	=	products of inertia about body x,y, and z axes
l_{ref}	=	reference length, ft
L	=	rolling moment, lb-ft
M	=	pitching moment, lb-ft
MR	=	momentum ratio of BSM jets to freestream
N	=	yawing moment, lb-ft

---

* Senior Aerospace Engineer, Associate Fellow, AIAA.
† Senior Aerospace Engineer, Vehicle Analysis Branch, Member AIAA.
‡ Aerospace Engineer, Analytical Mechanics Associates, Inc, Hampton VA, Member AIAA.
§ Aerospace Engineer, Vehicle Analysis Branch, Senior Member AIAA.
** Aerospace Engineer, Analytical Mechanics Associates, Inc, Hampton VA, Member AIAA.
†† Aerospace Engineer, Vehicle Analysis Branch, SACD, Associate Fellow AIAA.

p,q,r = angular velocity components in body axes, deg/s
q_∞ = freestream dynamic pressure, lb/ft^2
R = radial location of SRB reference point in SSME plume coordinate system, ft
S_{ref} = reference area, ft^2
$\mathbf{T}_A^{(CON)}, \mathbf{T}_B^{(CON)}$ = joint constraint torque vector for body A and B

V_∞ = freestream velocity, ft/s
X_b, Y_b, Z_b = coordinates in SRB body axes system, ft
$\Delta x, \Delta y, \Delta z$ = relative axial, lateral and normal distances during separation, ft
α = angle of attack, deg
β = angle of sideslip, deg
$\Delta\alpha$ = α(SRB) – α(OET), SRB and OET relative difference in angle of attack, deg
$\Delta\beta$ = β(SRB) – β(OET), SRB and OET relative difference in sideslip, deg
γ = flight path angle, deg
θ,ϕ,ψ = Euler angles in pitch, roll and yaw, deg
ρ_∞ = freestream density, slugs/ft^3
σ = standard deviation

Suffixes
b = body axes system
f = isolated or freestream conditions
p = SSME plume impingement

Acronyms
ADAMS® = Automatic Dynamic Analysis of Mechanical Systems
AEDC = Arnold Engineering Development Center
BSM = Booster Separation Motor
CG = Center of gravity
ConSep = Conceptual Separation
ET = External Tank
LSRB = Left Solid Rocket Booster
MRC = Moment reference center
NASA = National Aeronautics and Space Administration
NGLT = Next Generation Launch Technology
OET = Orbiter + ET
POST 2 = Program to optimize simulated trajectories II
RSRB = Right Solid Rocket Booster
SEE = Synergistic Engineering Environment
SRB = Solid Rocket Booster
SSME = Space Shuttle Main Engine
SSTO = Single-Stage-To-Orbit
STS = Space Transportation System
SVDS = Shuttle Vehicle Dynamic Simulation
TSTO = Two-Stage-To-Orbit

I. Introduction

The problem of dynamic separation of multiple bodies within the atmosphere is complex and challenging. One problem that has received significant attention in literature is that of store separation from aircraft[1]. A similar example is the separation of the X-15 research vehicle from the B-52 carrier aircraft.[2] In both of these cases, the store and the X-15 vehicle are much smaller in size than the parent vehicle. The other class of stage separation problem involves separation of two vehicles of comparable sizes (as in the case of multi-stage reusable launch vehicles) where the integrity of each stage is important after separation. A method for computing 6 DOF trajectories

of hinged/linked vehicles is presented in Ref. 3 and Ref. 4 presents a summary of stage separation capabilities in the 1960s and 70s.

NASA studies on stage separation of multi-stage reusable launch vehicles date back to the 1960s.[5-9] More recently, Naftel et al[10-12] considered staging of two wing-body vehicles. NASA's Next Generation Launch Technology (NGLT) Program identified stage separation as one of the critical technologies needed for the successful development and operation of next generation multi-stage reusable launch vehicles[13]. In response to this directive, the stage separation analysis and simulation tool called ConSep (Conceptual Separation) was developed as a part of this activity.[14] ConSep is a MATLAB® based wrapper to the ADAMS® solver which is an industry standard commercial software for solving dynamics problems involving multiple bodies connected by joints. Applications of ConSep for two-body (Bimese TSTO) and three-body (Space Shuttle solid rocket booster) separations are discussed in Refs. 14 and 15. For performing seamless end-to-end simulations of complete launch vehicle trajectories including stage separation, as recommended by the X-43 A (Hyper-X) Return-To-Flight Review Board[16], ADAMS® has to be linked to a trajectory simulation code like the Program to Optimize Simulated Trajectories (POST) to model internal forces and moments at joints that connect multiple vehicles. However, linking ADAMS® (Ref. 17) with POST is not advantageous because ConSep uses only a very small fraction of ADAMS® capabilities and it significantly increases POST run times for quick conceptual level studies.

In Refs. 18 and 19, the Constraint Force Equation methodology (CFE) for modeling internal constraint forces and moments due to simple joints connecting multiple bodies was developed and its implementation in POST2 was discussed. The CFE methodology in POST2 provides a framework for computing the internal constraint forces and moments exerted across various joints and applying them as external loads on each vehicle. Thus, the problem of motion of multiple bodies connected with joints is reduced to one of multiple free body motion with these additional external forces and moments. Consequently, such motions can be simulated with POST2. Thus, with CFE implementation, POST2 can be used to perform an efficient end-to-end simulation of launch vehicle trajectories, including stage separations. The CFE methodology was tested extensively in a stand-alone mode, using several test cases involving fixed, revolute and universal joints. These results were in good agreement with those using ADAMS® and Autolev[20] (another industry standard software for simulation of motion of multi-bodies connected with joints). The CFE/POST2 implementation was also applied to the separation of the Hyper-X Research Vehicle (X-43A) from the Pegasus Booster and the results compared well with the flight test data.[19]

In this paper, CFE/POST2 is applied to a more complex problem of three-body separation, namely that of Space Shuttle solid rocket booster (SRB) separation from the Orbiter and External Tank (OET), and the results are compared with STS-1 flight test data.[21-23] In this study, only the separation of the SRB from the OET was simulated. The end-to-end Space Shuttle trajectory from lift-off to orbit insertion and Orbiter re-entry were not addressed.

II. Constraint Force Equation Methodology

To illustrate the basic concept of the CFE methodology, consider the motion of two rigid bodies A and B connected by a single joint as shown in Fig. 1. The external forces ($\mathbf{F}_A^{(EXT)}$ and $\mathbf{F}_B^{(EXT)}$) and torques ($\mathbf{T}_A^{(EXT)}$ and $\mathbf{T}_A^{(EXT)}$) are the resultants of gravity, aerodynamic, and propulsive forces on each vehicle and are routinely computed by POST2. Figure 1(b) shows the internal constraint forces and moments ($\mathbf{F}^{(CON)}$ and $\mathbf{T}^{(CON)}$) that are computed by CFE and act on each vehicle at the joint location. These internal forces and moments constrain the way in which one vehicle can move relative to the others, and are dependent upon the external forces acting on each vehicle as well as the type of joint. For joints that permit only relative rotation between two bodies, the forces and moments on one body are equal and opposite to those acting on the other body, as shown. Finally, the free body diagram shown in Fig. 1(c) and the flow chart shown in Fig.2 illustrate the way in which CFE is implemented in POST2. At each integration time step, the current version of POST2 computes all the external forces and moments acting on each vehicle. The CFE routine works in parallel and computes the internal constraint forces and moments required to satisfy the constraints imposed by the joint. Next, these internal joint loads are applied to each vehicle as additional external forces and moments, and the POST2 solution is propagated in the usual manner to the next time step. Thus, the net external forces and moments on each vehicle are the sum of the usual external forces and moments and the joint loads, applied to each vehicle as additional external forces and moments. Consequently, the CFE simply augments the vehicle external loads and does not require modification to the POST2 equations of motion. The relative displacement between the joint locations is computed at every integration step and is used as a measure of how well CFE satisfies the constraint. Additional information on CFE methodology is available in Refs 18 and 19.

III. Space Shuttle: Vehicle Description

The Space Shuttle is designed to launch a variety of payloads into (and/or retrieve from) Earth orbit. The Shuttle can deliver up to 65,000 lb for an easterly launch from the Eastern Test Range at Kennedy Space Center (KSC) and up to 32,000 lb for a polar orbit launch from the Western Test Range at Vandenberg Air Force Base. The Shuttle launch configuration consists of the Orbiter, External Tank (ET) and the two SRBs. A schematic arrangement of the launch configuration is shown in Fig. 3.

The burn time of the SRBs is approximately two minutes. At burn out, the left and right SRBs separate simultaneously. The nominal staging of SRBs occurs from 150,000 ft to 180,000 ft altitude and Mach 3.75 to 4.0. The SRB lateral and vertical separation is aided by a cluster of four booster separation motors (BSMs) located in the forward pods and another cluster of four BSMs on the aft skirts of each SRB. The BSMs provide lateral and normal acceleration of the SRBs away from the OET. The relative axial acceleration is achieved by the thrust from the SSMEs. After separation, the SRBs are decelerated by parachutes during their descent for splashdown in the ocean, approximately 141 nautical miles from the launch site. The SRBs are recovered and are refurbished for reuse. A schematic illustration of SRB separation, descent and recovery is presented in Fig. 4.

The SRBs are attached to the ET at one point on the forward end and at three points on the aft end. The forward attachment point is used to transfer the thrust loads from the SRB to the ET. The aft attachment points consist of three struts. At SRB separation, the bolts holding the forward and aft attachment points are severed, the aft joints are released, and the SRBs rotate about the forward joints by approximately 1 deg prior to release. Simultaneously, the forward and aft BSMs on each SRB are fired. The BSMs burn for about 0.7 sec. The SRB separation is complex and is influenced by several factors. The OET cannot make a lateral maneuver to aid separation because an SRB is coming off each side. Consequently, the OET is flown straight and in attitude-hold mode. Because the Orbiter engines are significantly above the OET center of gravity, they need to be canted for achieving moment balance for attitude-hold mode as shown in Fig. 5(a). As a result, the OET moves in z-direction towards the SRBs. The BSMs have sufficiently high thrust to move the SRBs away from the OET, resulting in a safe separation.

The nominal mass and inertia at SRB separation for STS-1 are given in Table I (Refs. 21-23). The center of gravity locations and aerodynamic moment reference points are shown in Fig. 5. During SRB separation, the thrust produced by each SSME was assumed to be equal to 467,000 lb, and the net thrust was assumed to pass through the center of gravity of the OET to reflect the "attitude hold" mode of the OET. The canting angle of the net thrust was estimated to be 13.35 deg as shown in Fig. 5(a).

The flight parameters at SRB separation for STS-1 are presented in Table II. The SRB propulsion characteristics for STS-1 are given in Table III. It may be noted that Ref. 23 gives the thrust values of 18,297.0 lb (left SRB) and 24049.0 (right SRB) for STS-1 at separation but time history of thrust tail-off is not presented. On the other hand, Ref. 23 gives the time history of nominal SRB thrust tail-off for the SRB separation sequence and these data are used in this paper. The time history of nominal thrust tail off from the initiation of SRB separation (with a 6 sec delay from separation cue) is shown in Fig. 6. The BSM nominal locations are presented in Table IV. Each of these BSM jets are nominally inclined 40 deg in the pitch plane and 20 deg in the roll-yaw plane as shown in Fig. 7. The variations in BSM cluster orientations from their nominal values and the cluster propulsion characteristics for STS-1 are given in Table V.

IV. Aerodynamic Database

The Shuttle SRB separation aerodynamic database is comprised of three components: (i) an isolated aerodynamic database for each vehicle when they are in freestream conditions, (ii) proximity coefficients (increments in relation to freestream coefficients and including mated conditions) for each vehicle, and (iii) plume impingement forces and moments on the SRBs to account for SSME plume impingement when that happens. For this analysis, the isolated and plume impingement aerodynamic characteristics for the left and right SRBs were assumed to be identical with proper sign adjustment. Note that, when the SRBs are not subject to SSME plume impingement, these forces and moments are zero.

The relative orientations and location during separation are defined in Fig. 8. Here, Δx, Δy, and Δz are orthogonal displacements of SRB from its mated position. The variable Δx is measured positive aft, Δy is positive outboards, and Δz is positive downward. For the mated position, $\Delta\alpha = \Delta\beta = \Delta x = \Delta y = \Delta z = 0$. The relative angles of attack and sideslip are defined as, $\Delta\alpha = \alpha(\text{SRB}) - \alpha(\text{OET})$ and $\Delta\beta = \beta(\text{SRB}) - \beta(\text{OET})$.

The proximity aerodynamic coefficients depend on eight variables α, β, $\Delta\alpha$, $\Delta\beta$, Δx, Δy, Δz and MR. The BSM jet momentum ratio (MR) was evaluated using the data given Table V and Figs. 8 and 9. The MR was found to be in

excess of 730. However, the hypercube proximity aero data goes up only to MR = 222.3. Therefore, when MR>222.3, using the "no extrapolation" approach recommended in Ref. 21, data for MR = 222.3 was used. At BSMs burn out, MR=0 and the power-off proximity data was used. Since the staging maneuvers last only for few seconds, the Mach number is usually assumed constant. The SSME plume impingement forces and moments depend on four variables A, R, θ, and ψ as shown in Fig. 10. Here, A and R are the axial and radial locations of the SRB reference point in SSME plume coordinate system, and θ and ψ are the pitch and yaw angles. The geometrical shape of the SSME engine plume was modeled using the data on the jet boundary given in Ref. 23. The plume impingement data[19] covers axial distances only up to 1700 in. For axial distances greater than 1700 in, the last value was held constant. The development of a proximity aerodynamic database for the Shuttle SRB separation was a difficult and complex task, because the number of data points needed to populate a conventional database with eight independent variables would be unusually large. To get around this difficulty, the Shuttle program developed a novel method called "hypercube[24], which used far fewer data points. This method allowed data to be placed only along required separation paths. For each selected Δx, two 4-dimensional hypercubes were situated to cover all anticipated trajectory values in Δy, Δz, $\Delta\alpha$, and $\Delta\beta$. The inner hypercube was designed to include nominal separation trajectories with 3σ dispersions, and the outer cube was designed to encompass all dispersions, including SSME failures. These hypercubes were not constrained to have parallel opposite sides. A nominal trajectory through hypercube space is schematically illustrated in Fig. 11. The range of variables in hypercube data is shown in Table VI and aerodynamic reference parameters are listed in Table VII. Additional information on the hypercube concept may be found in Ref. 19. The aerodynamic forces and moments during separation are defined as

$$F_{0,i} = \frac{\rho}{2} V_\infty^2 S_{ref} \left(C_{0f,i} + \Delta C_{0f,i} \right) + F_{p0,i} \tag{1}$$

$$T_{0,i} = \frac{\rho}{2} V_\infty^2 S_{ref}\, l_{ref} \left(C_{0t,i} + \Delta C_{0t,i} \right) + T_{p0,i} \tag{2}$$

where, $C_{0t,i}$ and $\Delta C_{0t,i}$ are any one of the three isolated or proximity force coefficients (axial, normal or side force) $C_{0t,i}$ and $\Delta C_{0t,i}$ are any of the three moment coefficients(pitching, rolling and yawing) and, i = 1,2,3 for right SRB, OET and left SRB respectively.

To verify proper implementation of the hypercube interpolator, Ref. 24 provides one check case. The input variables for this check case are: $\alpha = 1.0$ deg, $\beta = 4.0$ deg, $\Delta x = 186.0$ in, $\Delta y = 65.0$ in, $\Delta z = 133.0$ in, $\Delta\alpha = -4.4$ deg, $\Delta\beta = -0.9$ deg, and MR = 196.1634. Present results are in good agreement with that check case as shown in Table VIII. This exercise indicates that both the hypercube interpolator routine and the proximity aerodynamic coefficients were properly implemented in this study. However, it may be noted Ref. 24 specifies MR = 200 for this check case but a detail verification indicated that the value of MR=196.1634 better matches all the other parameters for this check case including the aerodynamic coefficients.

The ConSep/ADAMS results (Ref 15) were based on modeling the proximity aerodynamic coefficients, using a response surface method, because the hypercube interpolator was not available at that time. Since a hypercube interpolator is the recommended approach, the ConSep results included in this paper were recomputed using the hypercube interpolator.

The isolated aerodynamic coefficients for each vehicle and the plume impingement forces and moments were obtained from the Space Shuttle Launch vehicle databook (Ref. 24). The proximity data tables and the hypercube interpolator routines were provided by Hoff and Paget (Ref. 25).

The CFE/POST2 simulation inputs include the following: (i) definition of body-fixed coordinate systems for each vehicle in relation to the selected ground-fixed (inertial) system, (ii) mass, inertia, and center of gravity of each of the three vehicles in respective body-fixed coordinate system, (iii) initial altitude, velocity and flight path angle, (iv) initial angle of attack of each vehicle, (v) proximity aerodynamic data tables and hypercube interpolator routines, (vi) isolated (freestream) aerodynamic coefficients, (vii) plume impingement forces and moments, (viii) aerodynamic reference parameters for each vehicle, (ix) thrust magnitudes and orientations for each of the forward and aft BSMs for both right and left SRBs, (x) thrust magnitudes for each SSME. The time/event for the release of front and aft joints, and the time for starting and

stopping the integration of equations of motion and step size, are presented in Table IX. Each aft joint was modeled as a fixed joint, released instantaneously, and each forward joint was modeled as a revolute joint that released when the SRBs rotated by 1 deg with respect to mated condition. The effect of forces in the attachment hardware at SRB release were not included in CFE/POST 2 simulation because the current version of CFE does not support preloaded joints.

The results of CFE/POST for STS-1 SRB separation are presented in Figs. 12 to 18 along with STS-1 flight data, Rockwell/Boeing SVDS (Shuttle Vehicle Dynamic Simulation), and ConSep simulation results.[15,22] The predicted relative locations of the vehicles during separation are in good agreement with the flight data (Fig. 12). However, differences exist in the lateral and vertical separation distances Δy and Δz. In the present ConSep and CFE/POST2 simulations, the estimated SSME thrust orientations (Fig. 5a) were used and it is possible that for STS-1 flight, there could be variations from these values and these factors directly contribute to observed differences in Δy and Δz. The component accelerations for OET and for the left and right SRBs are in good agreement with the flight data (Figs. 13 to 15). However, the component angular velocities show differences from the flight data (Figs. 16 to 18) and the reasons for these differences are not clear. The gimbal angles of each of the three SSME were continuously varied during separation in STS-1, and these variations were not modeled in CFE/POST and ConSep. Furthermore, strut forces acting at the aft joint at release were not included, and, the rolling moment coefficient for each SRB was set equal to zero. It is possible that such factors contribute to these differences.

The Synergistic Engineering Environment[26] (SEE) was used to create animations of the staging maneuvers. The SEE used the geometry models of the SRBs, OET, and the time history of trajectory variable to generate these animations. The BSM plume shapes were computed using the data of Ref. 21 and were included in SEE animation for the duration of their burn (0.68 sec). The SSME plumes are on for the entire 4 sec duration. Some sample snapshots of SEE animation are presented in Fig. 19. It is interesting to note that the SSME plume impinges on the SRBs for $t > 3.0$ sec.

V. Concluding Remarks

The constraint force equation (CFE) methodology provides a framework for modeling constraint forces and moments acting at joints that connect multiple vehicles. With implementation in POST II, the CFE provides a capability to simulate end-to-end trajectories of launch vehicles including stage separation. The POST/CFE simulation methodology was applied to the STS-1 SRB separation as a further test and validation case for CFE/POST2. The results compare fairly well with flight data and this exercise serves as a test/validation for the CFE/POST 2 algorithm. With this validation, the CFE/POST 2 can be used for end-to-end simulation of launch vehicle trajectories, including stage separation, for system level studies.

VI. Acknowledgments

The authors would like to acknowledge Johann Hoff and Scott Paget for providing SRB separation documentation, proximity aerodynamic data tables hypercube interpolation routines, and Scott Angster for SEE animations.

VII. References

[1]Dillenius, M.F.E., Perkins, S.C., and Nixon, D., *Pylon Carriage and Separation of Stores*, AIAA Progress in Astronautics and Aeronautics: Tactical Missile Aerodynamics-General Topics, M.J.Hemsch, ed., Vol. 141, 1992.

[2]Taylor, R.T., and Alford, W.J., Jr., A wind tunnel investigation of the carry loads and mutual interference effects of 1/40-scale models of the X-15 and B-52 airplanes in combination, NASA TM X-184, December 1959.

[3]Hurley, M.J., *"Digital Program P5255, A Six-Degree, Multiple Body Separation Simulation for Hinged and/or Linked Lifting Entry Vehicles"*, Vols. I and II, GDC-ERR-1377, December 1969, Convair Aerospace Division of General Dynamics, San Diego, CA.

[4] Hurley, M.J., Carrie, G.W., "Stage Separation of Parallel-Staged Shuttle Vehicles: A Capability Assessment," Journal of Spacecraft, Vol. 9, No. 10, October 1972, pp. 764-771.

[5]Decker, J.P., and Wilhite, A.W., *Technology and Methodology of Separating Two Similar Size Aerospace Vehicles Within the Atmosphere*. AIAA Paper 1975-29, Jan. 1975.

[6]Decker, J.P., *Experimental Aerodynamics and Analysis of the Stage Separation of Reusable Launch Vehicles*. NASA-SP-148, January 1967.

[7]Decker, J.P., and Gera, J., *An Exploratory Study of Parallel-Stage Separation of Reusable Launch Vehicles*. NASA TN D-4765, October 1968.

[8]Decker, J.P., *Aerodynamic Interference Effects Caused by Parallel-Staged Simple Aerodynamic Configuration at Mach Numbers of 3 and 6*. NASA TN D-5379, Aug. 1969.

[9]Wilhite, A.W., *Analysis of Separation of the Space Shuttle Orbiter from a Large Transport Airplane*. NASA TM X-3492, June 1977.

[10]Naftel, J.C., and Wilhite, A.W., *Analysis of Separation of a Two-Stage Winged Launch Vehicle*. AIAA Paper 86-0195, Jan. 1986.

[11]Naftel, J.C., and Powell, R.W., *Aerodynamic Separation and Glideback of a Mach 3 Staged Orbiter*. AIAA Paper 90-0223, Jan. 1990.

[12]Naftel, J.C., and Powell, R.W., *Analysis of the Staging Maneuver and Booster Glideback Guidance for a Two-Staged, Winged, Fully Reusable Launch Vehicle*. NASA TP-3335, 1993.

[13]Murphy, K.J., Buning, P.G., Pamadi, B.N., Scallion, W.I., and Jones, K.M.; *Status of Stage Separation Tool Development for Next Generation Launch Vehicle Technologies*. AIAA Paper 2004-2595.

[14]Pamadi, B.N., Neirynck, T.A., Covell, P.F., Hotchko, N.J., and Bose, D.M., *Simulation and Analyses of Two-Stage Reusable Launch Vehicles,* Journal of Spacecraft and Rockets, Vol. 44, No. 1, January-February 2007, pp. 66-80.

[15]Pamadi, B.N., Hotchko, N.J., Jamshid Samareh, Covell, P.F., and Tartabini, P.V., *Simulation and Analyses of Multi-Body Separation in Launch Vehicle Staging Environment,* AIAA Paper 2006-8083.

[16]Reubush, D.E., Nguyen, L.T., and Rausch, V.L., "*Review of X-43A Return to Flight Activities and Current Status*," AIAA 2003-7085.

[17] "Using ADAMS/Solver", Mechanical Dynamics Inc., 1999.

[18]Toniolo, M. D., Tartabini, P.V., Pamadi, B.N., and Hotchko, N.J., *Constraint Force Equation Methodology for Modeling Multi-Body Stage Separation Dynamics,* AIAA Paper 2008-219.

[19]Tartabini, P.V., Roithmayr, C., Karlgaard, C., Toniolo, M.D., and Pamadi, B.N., *Verification of Contstraint Force Equation Methodology for Modeling Multi-Body Stage Separation,* AIAA Paper 2008-, AIAA Flight Mechanics Conference, Honolu, Hawaii, August, 2008.

[20]Kane, T. R., and Levinson, D. A., Autolev 4 User's Manual, OnLine Dynamics, Inc., Sunnyvale, CA, 2005.

[21]"*Space Shuttle SRB Separation Databook",* Dopcument No. SSD97D0385, Boeing North American Inc., Septermber 30, 1997.

[22] STS 81-0277 "*Space Shuttle System Engineering Analysis Report, SRB Separation System Verification,*" Rockwell International, March 1981.

[23] STS 82-0570, "*Space Shuttle System SRB Separation Verification For Operations,*" Rockwell International, November 1982.

[24]"Aerodynamic Design Data Book, Vol. 2, Launch Vehicle", SD72-SH-0060, Volume 2L, Rockwell International, June 1981.

[25]Bornemann, W.E., "Substantiation of New Hypercube Interpolator (DMS 290-200-434), No. SAS/AERO/83-113, Rockwell International Internal Letter dated March 9, 1983.

[26] Angster, S., *Synergistic Engineering Environment Build II User's Guide Revision E*, AMA Report No. 03-31, Analytical Mechanics Associates, Hampton, VA, August 2003.

Table I. Vehicle Mass and Inertia Properties at Staging (Ref. 22)

Configuration	Weight, lb	Ixx, Slugs ft^2	Iyy, Slugs ft^2	Izz, Slugs ft^2	Ixy, Slugs ft^2	Iyz, Slugs ft^2	Ixz, Slugs ft^2
Orbiter/+ET	1,473,332	5,241,320	83,826,248	80,221,300	124,263.3	–12,024,025.0	35,820.9
Left SRB	180,881	192,915	11,348,219	11,351,222	–27,923.0	7,508.0	688.0
Right SRB	181,833	241,702	11,463,621	11,466,376	24,651.0	9,670.0	–1,043.0

Table II. Flight Parameters at SRB Separation for STS-1 (Ref. 22)

Parameter	Value
Altitude, ft	173,857
Velocity, ft/sec	4112.0
Mach Number	3.877
Dynamic Pressure, lb/ft^2	12.83
Angle of Attack, deg	3.0
Sideslip, deg	0.75
Flight Path Angle, deg	36.966
Body Roll Rate, deg/sec	–0.3
Body Pitch Rate, deg/sec	0.4
Body Yaw Rate, deg/sec	0

Table III. SRB Propulsion Characteristics at Separation, STS-1 (Ref. 22)

Parameter	Left SRB	Right SRB
Propellant Mean Bulk Temperature (PMBT), deg F	**68.0**	**68.0**
Pitch gimbal angle, deg	0.042	0.064
Yaw gimbal angle,deg	–0.679	0.672

Table IV. BSM Nominal Locations in SRB coordinates (Ref. 22)

BSM No	Type	Xb (inches)	Yb (inches)	Zb (inches)
1	Forward	290.230	19.625	26.616
2	Forward	303.888	20.811	30.863
3	Forward	290.23	2.351	32.772
4	Forward	303.888	3.896	37.019
5	Aft	1886.722	59.755	82.245
6	Aft	1886.722	40.573	93.418
7	Aft	1886.722	28.357	97.864
8	Aft	1886.722	15.548	100.682

Table V. Variations in BSM Orientations and Propulsion Characteristics at Separation (STS-1)

Parameter	Left SRB Forward	Left SRB Aft	Right SRB Forward	Right SRB Aft
$\Delta\phi$, deg	0.04	0.113	0.18	0.05

Δθ, deg	0	0.10	0.14	0.071
Maximum Chamber Pressure, psia	1844.9	1832.1	1854.7	1848.4
Maximum Thrust, lb	92,096.0	91,457.0	92,587.0	92,272.0
Average Thrust,l lb	89,620	88,162	90,776	90,884
Average Duration, sec	0.692	0.696	0.671	0.686

Table VI. Range of Independent Variables in Hypercube Proximity Aerodynamic Database

Plume-off (MR = 0)

α (deg)	β (deg)	Δx (inches)	Δy (inches)	Δz (inches)	Δα (deg)	Δβ (deg)
–10 to 10	**–10 to 10**	**0**	**0**	**0**	**0**	**0**
-10 to 10	**-10 to 10**	**100**	**10 to 110**	**40 to 250**	**–7.0 to 0**	**–5.5 to 1.0**
-10 to 10	**-10 to 10**	**300**	**30 to 260**	**40 to 550**	**–17.0 to 0**	**–15.0 to 2.0**
-10 to 10	**-10 to 10**	**600**	**90 to 510**	**140 to 800**	**–30.0 to 0**	**–20.0 to 3.0**
-10 to 10	**-10 to 10**	**1100**	**100 to 700**	**180 to 900**	**–33.0 to 0**	**–20.0 to 3.0**
-10 to 10	-10 to 10	1700	200 to 800	300 to 1000	–34.0 to –5.0	–20.0 to 8.0

Plume-on (MR = 133.4, 222.3)

α (deg)	β (deg)	Δx (inches)	Δy (inches)	Δz (inches)	Δα (deg)	Δβ (deg)
–10 to 10	–10 to 10	0	0	0	0	0
-10 to 10	-10 to 10	100	10 to 110	40 to 250	–7 to 0	–5.5 to 1.0
-10 to 10	-10 to 10	200	20 to 150	60 to 280	–7 to 0	–6.5 to 0.5

Table VII. Aerodynamic Reference Parameters

Vehicle	Reference Area	Reference Length	Moment Reference Point
Right SRB	2690.0 sq ft	107.525 ft	X=88.27, Y=0. Z=0 in SRB coordinate system with origin at nose
OET	2690.0 sq ft	107.525 ft	X=64.54 ft, Y=0, Z= 4.17 ft, in OET coordinate system with origin at nose
Left SRB	2690.0 sq ft	107.525 ft	X=88.27, Y=0. Z=0 in SRB coordinate system with origin at nose

Table VIII. Verification of Hypercube Interpolator Implementation

Aerodynamic Coefficient	Present Result	Check Case (Ref. 24)
CN_{OET}	-0.08119	-0.08117
Cm_{OET}	-0.07141	-0.0714
CY_{OET}	0.03983	0.03984
Cn_{OET}	-0.03674	-0.03674
Cl_{OET}	0.01277	0.01277
CN_{SRB}	0.00399	0.00399
Cm_{SRB}	0.00899	0.00899
CY_{SRB}	0.011	0.011
Cn_{SRB}	-0.0009	-0.0009

Table IX. CFE/POST 2 Simulation Parameters

Parameter	Value
Simulation time, sec	4.0
Integration step size, sec	0.001
Aft (fixed) joint release, sec	0.02
Front (revolute) joint release, deg	1.0

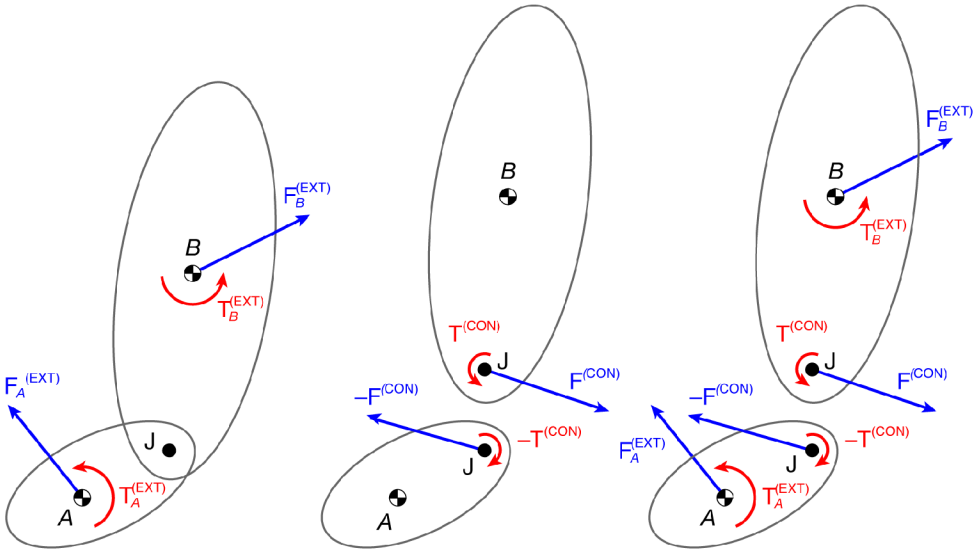

a) External forces. b) Internal forces. c) Free body diagram.

Figure 1. Decomposition of external forces and internal constraint forces to free body diagram solved by CFE method.

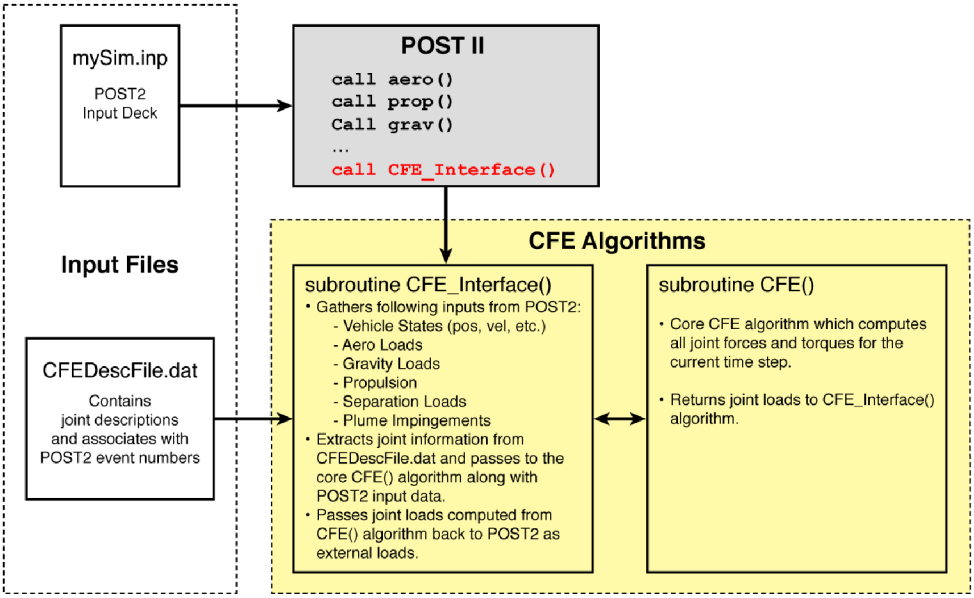

Figure 2. Schematic illustration of CFE implementation in POST II.

Charles P. Leonard 8/5/09 4:32 PM
Comment: legibility of yellow box is questionable, was not clear when printed.

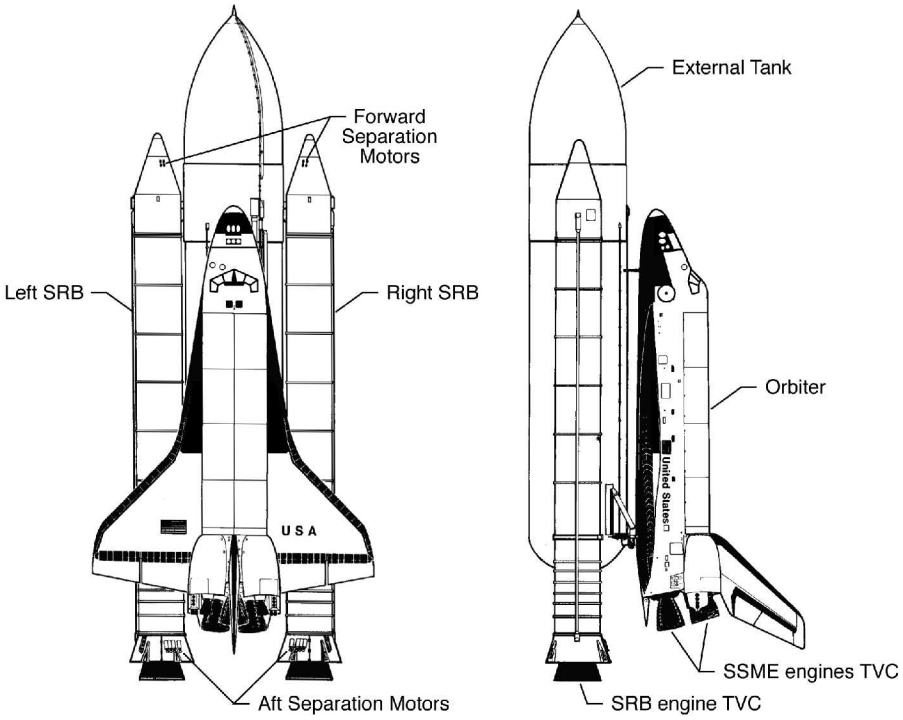

Figure 3. Space Shuttle vehicle configuration. (Ref. 20).

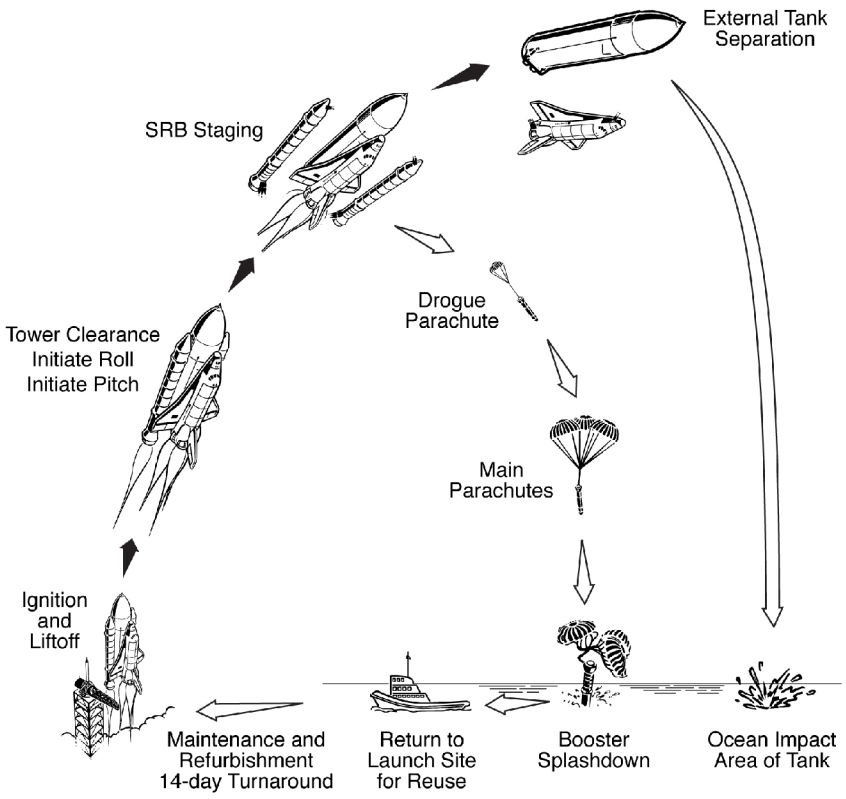

Figure 4. Schematic illustration of Space Shuttle staging events.

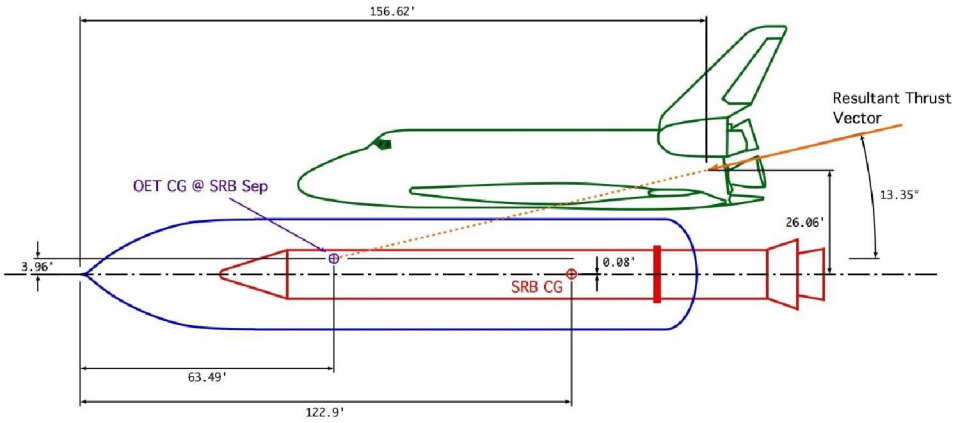

(a) Center of gravity locations

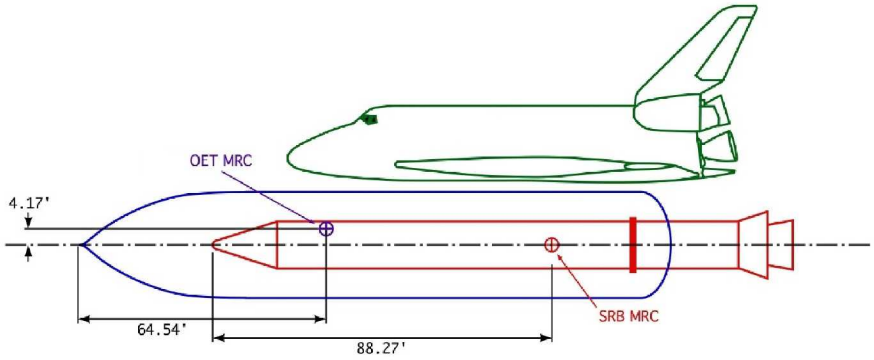

(b) Aerodynamic moment reference points.

Figure 5. Center of gravity and aerodynamic moment reference points for STS-1.

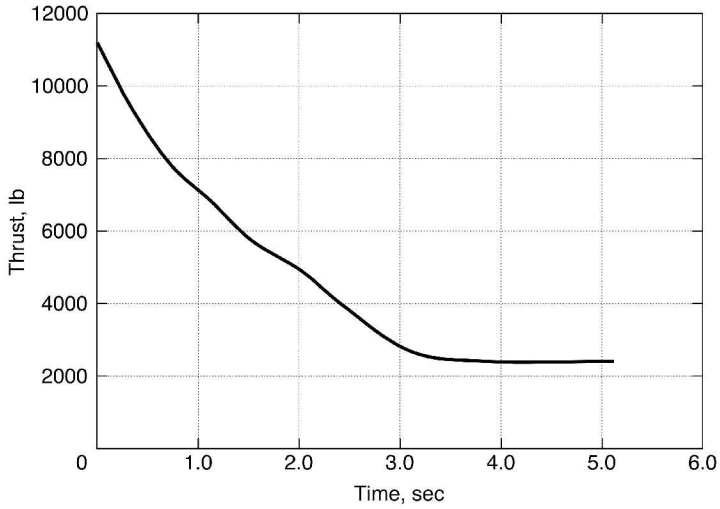

Figure 6. SRB thrust tail-off characteristics for STS-1.

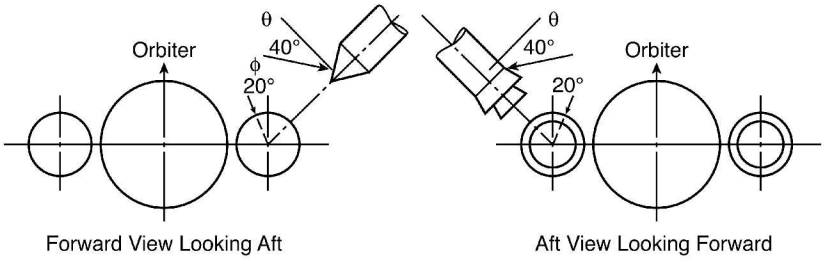

Figure 7. BSM cluster locations and orientations.

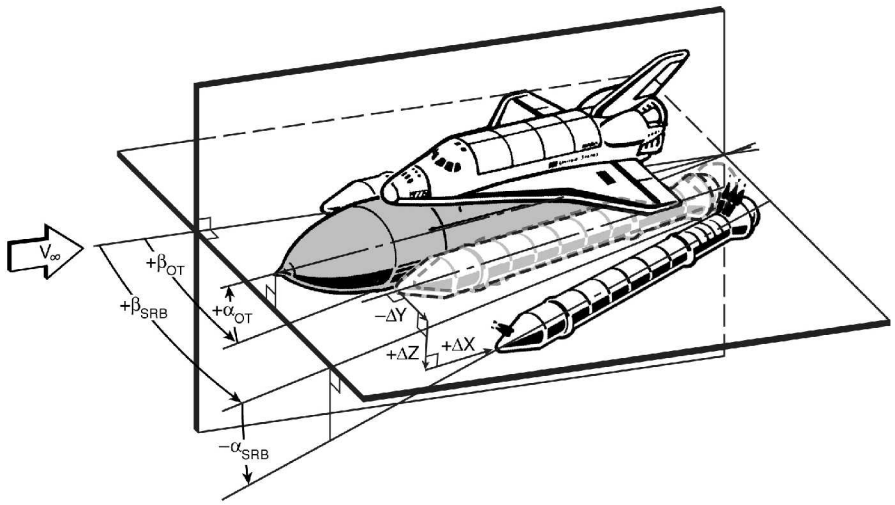

Figure 8. Relative orientations and locations during separation.

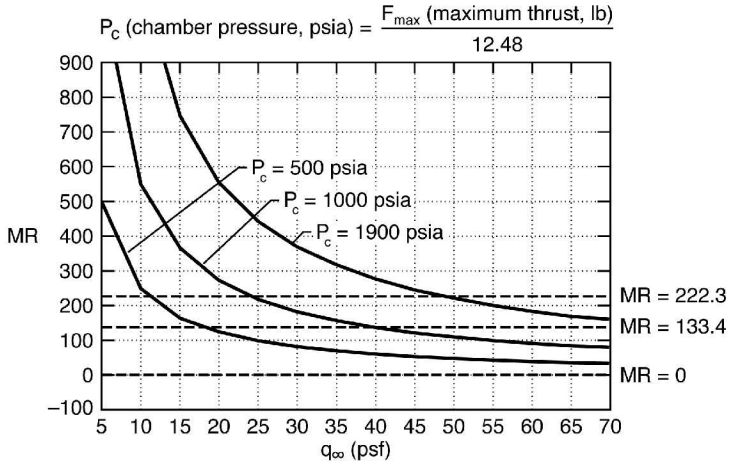

Figure 9. Variation of BSM jet momentum ratio with freestream dynamic pressure (Ref. 20).

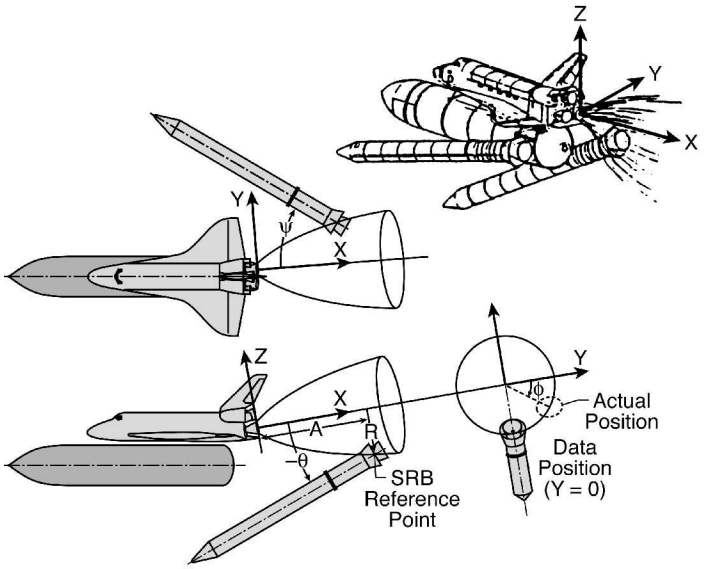

Figure 10. Schematic illustration SSME plume impingement coordinate system (Ref. 24).

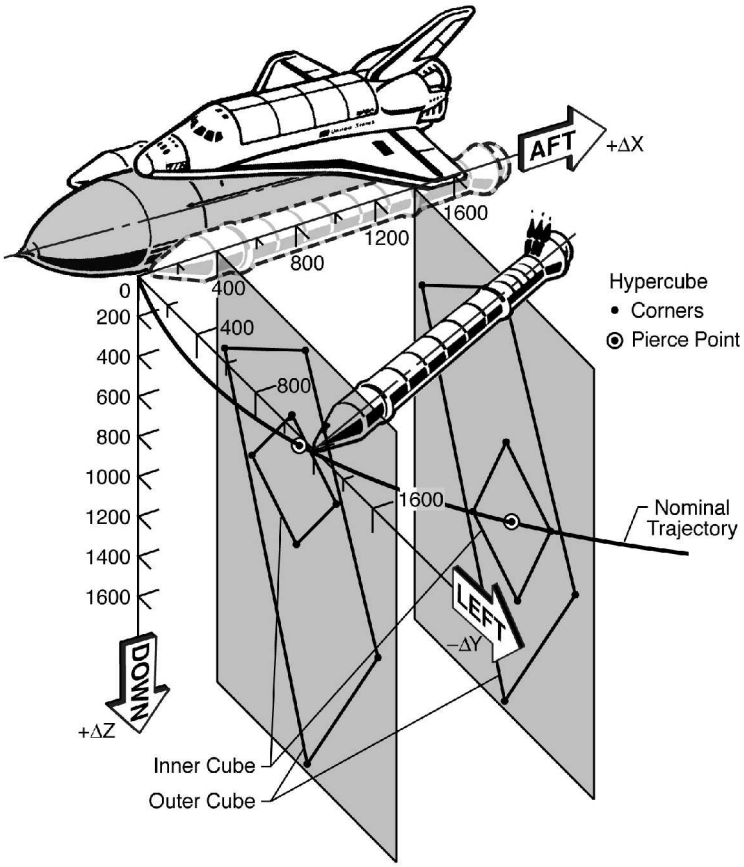

Figure 11. Hypercube data structure and nominal trajectory (Ref. 24)

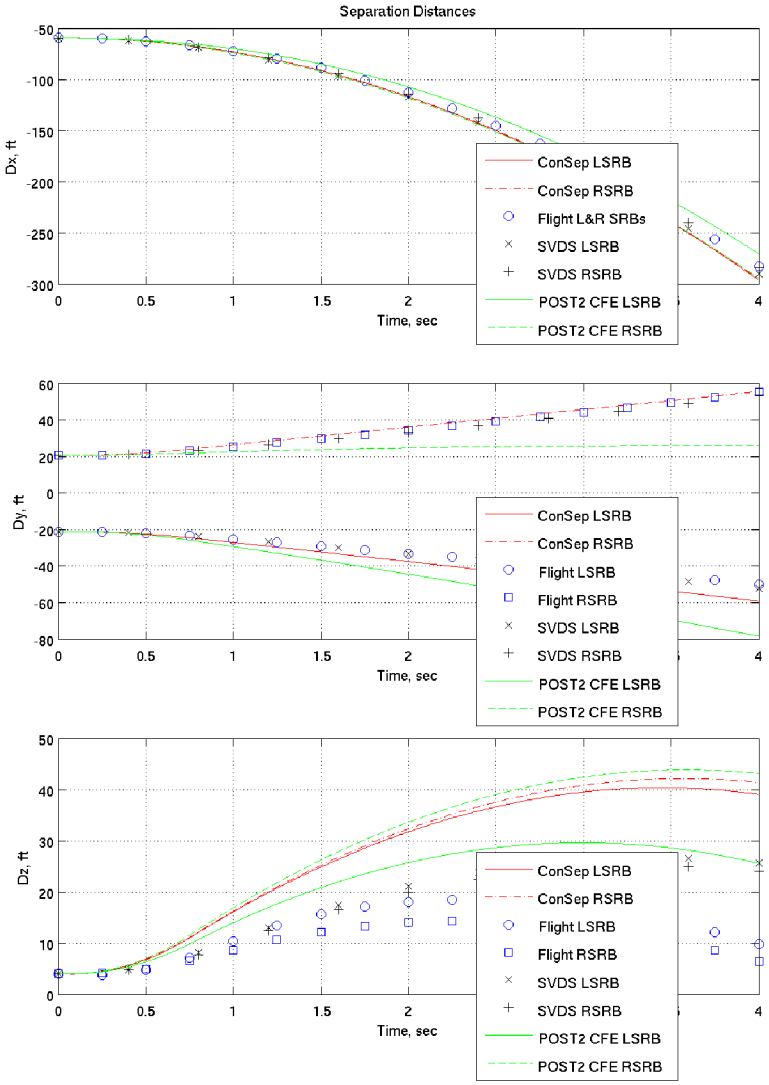

Figure 12. Variation of relative distances Δx, Δy and Δz with time during SRB separation, STS-1.

Charles P. Leonard 8/5/09 4:30 PM
Comment: move legends

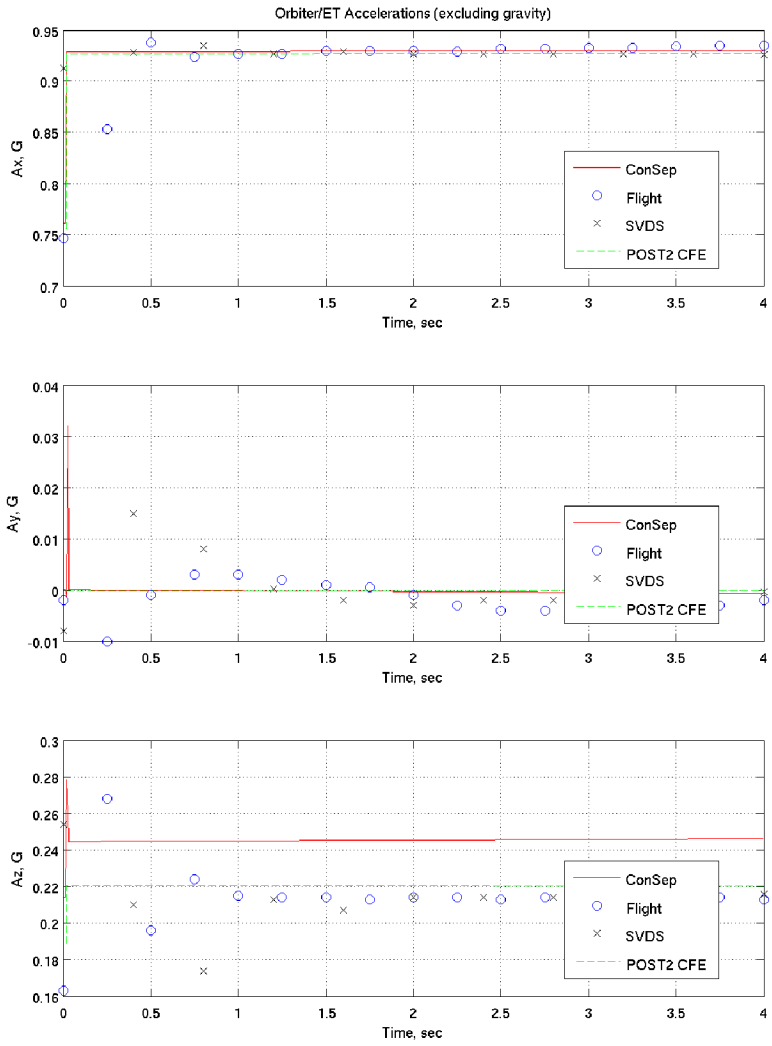

Figure 13. OET: Variation of acceleration components during separation, STS-1.

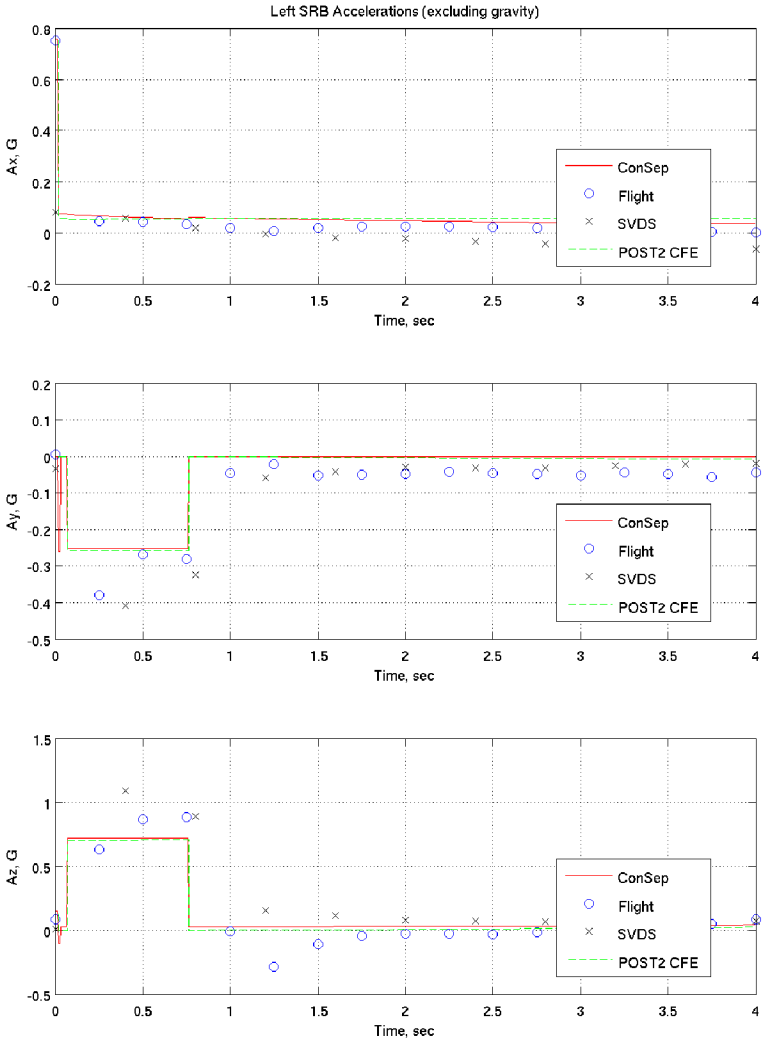

Figure 14. Left SRB: Variation of acceleration components during separation, STS-1.

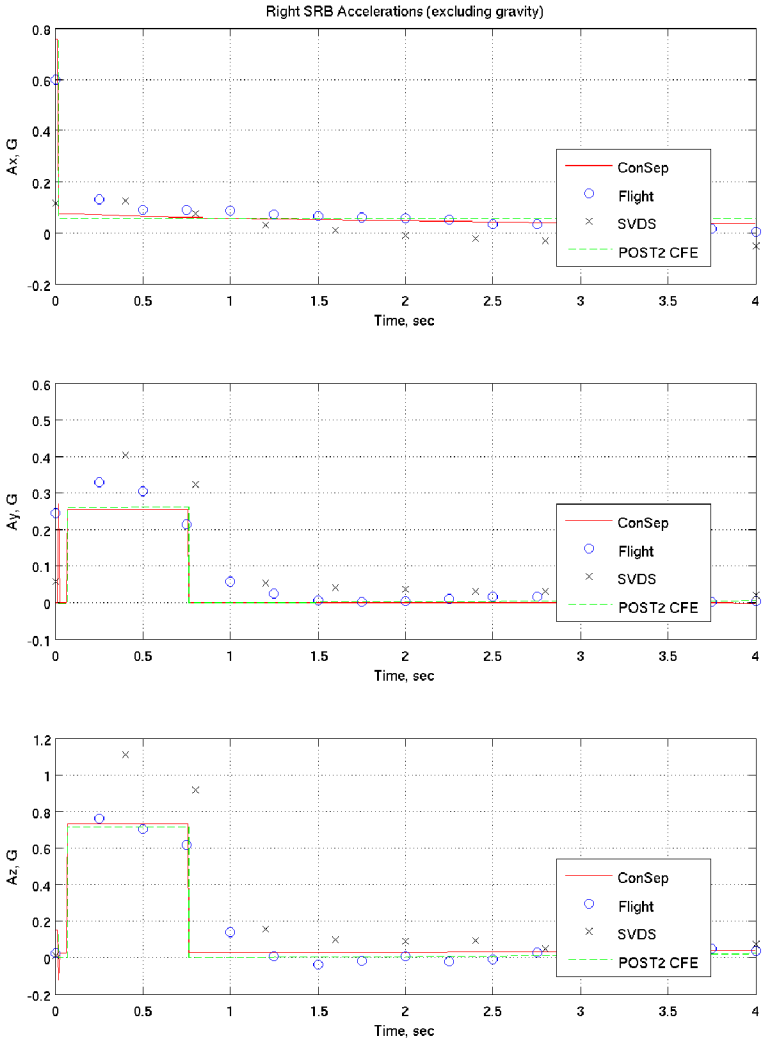

Figure 15. Right SRB: Variation of acceleration components during separation, STS-1.

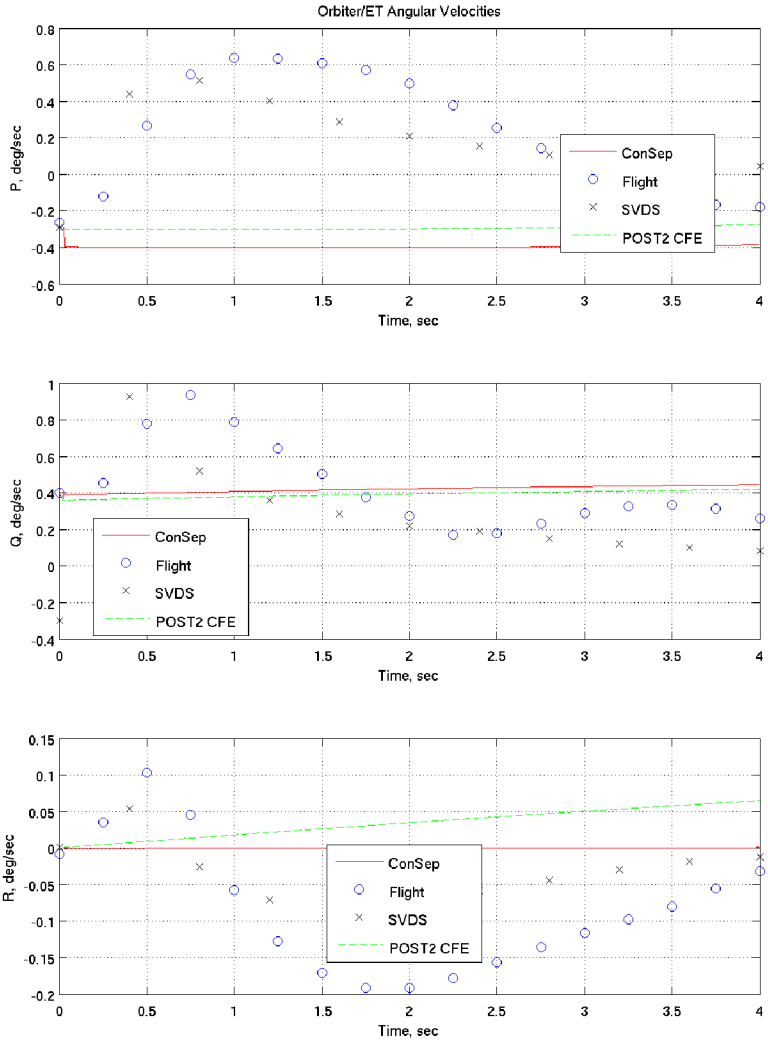

Figure 16. OET: Variation of angular velocity components during separation, STS-1.

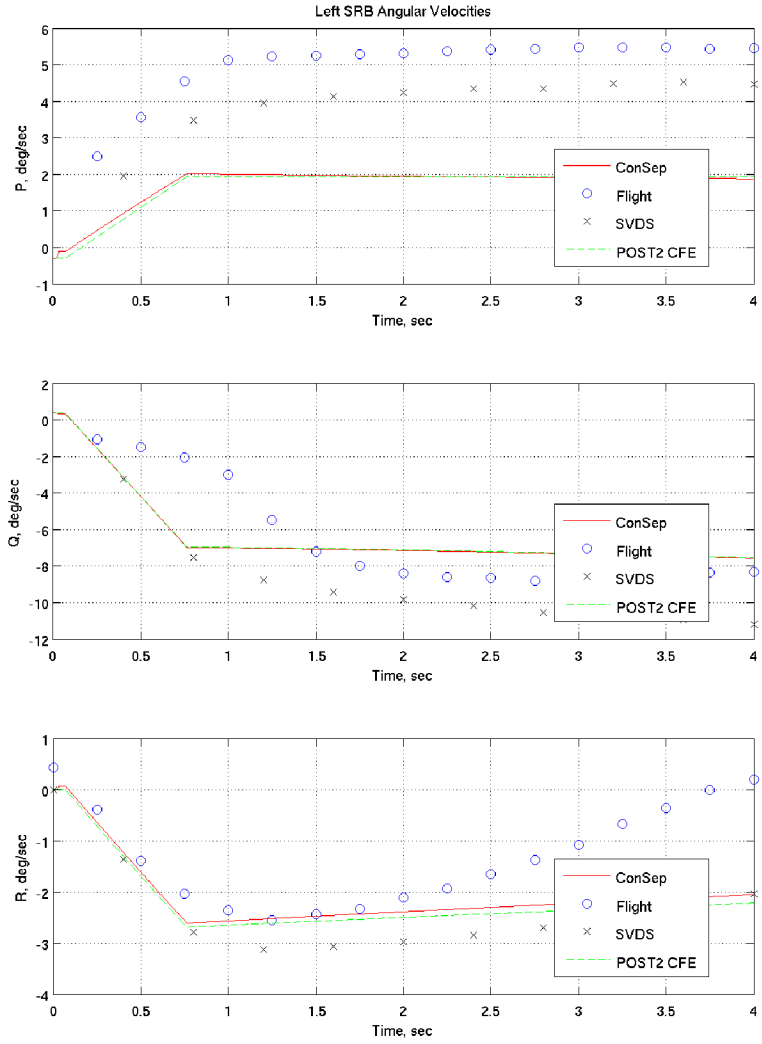

Figure 17. Left SRB: Angular velocity components during separation, STS-1.

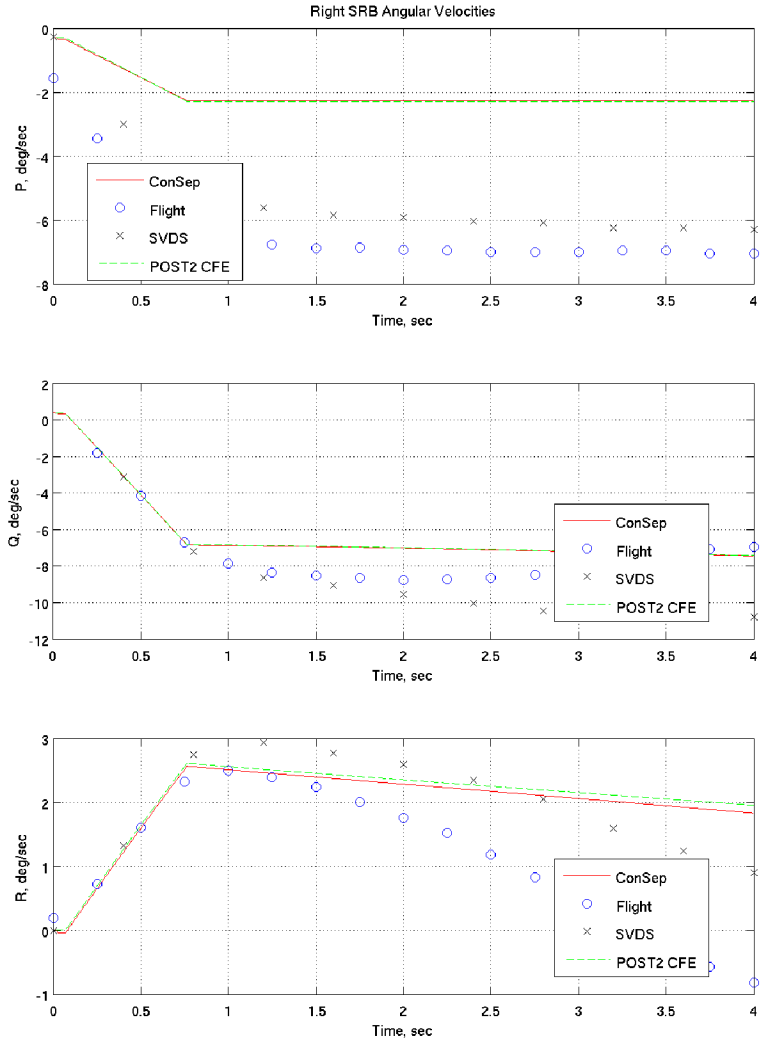

Figure 18. Right SRB: Angular velocity components during separation, STS-1.

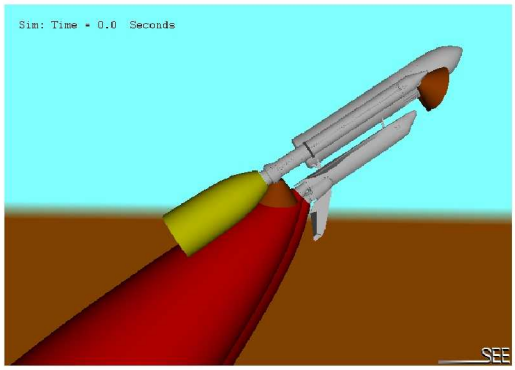

(a) t = 0.

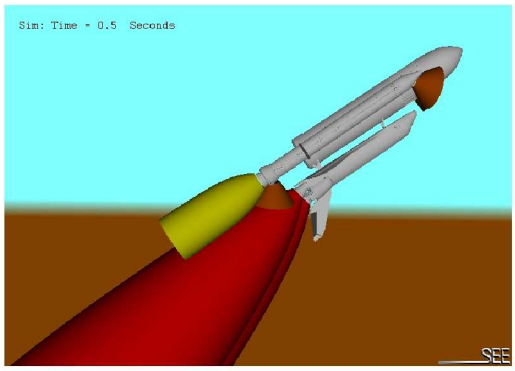

(b) t=0.5 sec

Charles P. Leonard 8/5/09 4:30 PM
Comment: some are bold, some are not

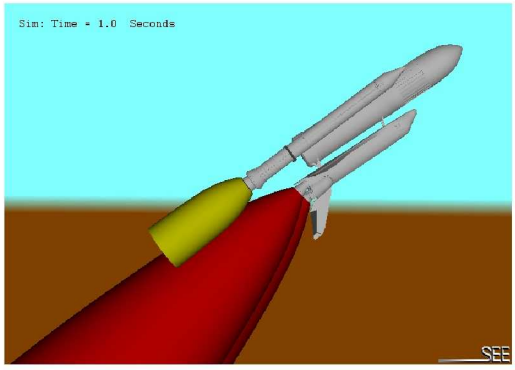

© t=1.0 sec

(d) t=1.5 sec

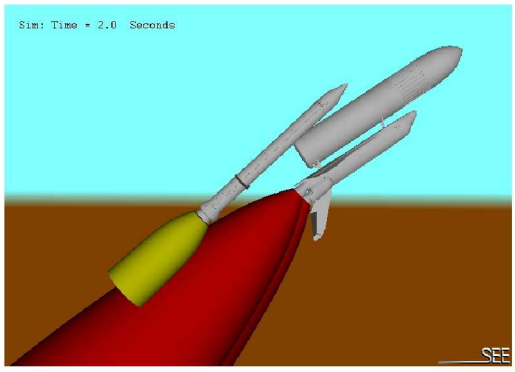

(e) t = 2.0 sec.

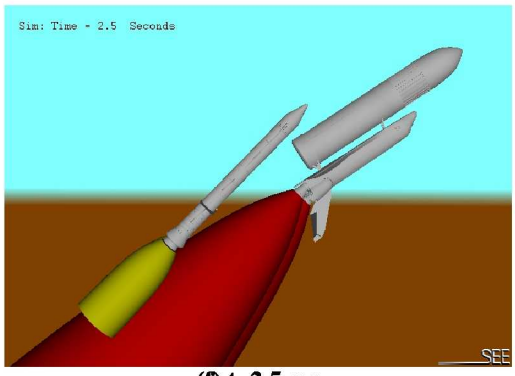

(f) t=2.5 sec

Figure 19. Snapshots of SEE animation